V International Conference on Computational Methods for Coupled Problems in Science and Engineering
COUPLED PROBLEMS 2013
S. Idelsohn, M. Papadrakakis and B. Schrefler (Eds)

AN ENHANCED IMMERSED STRUCTURAL POTENTIAL METHOD (ISPM) FOR THE SIMULATION OF FLUID-STRUCTURE INTERACTION PROBLEMS

ANTONIO J. GIL*, AURELIO ARRANZ CARREÑO*, JAVIER BONET* AND CLARE WOOD*

*Civil and Computational Engineering Centre (C^2EC)
College of Engineering, Swansea University
Singleton Park, SA2 8PP, Swansea, United Kingdom
e-mail: a.j.gil@swansea.ac.uk, web page:
http:///www.swan.ac.uk/staff/academic/engineering/gilantonio/

Key words: Fluid-Structure Interaction, Immersed methods, ISPM

Abstract. Immersed methods are widely used nowadays for the computational simulation of Fluid-Structure Interaction problems. In this paper, the Immersed Structural Potential Method (ISPM) is coupled with a Runge-Kutta-Chebyshev Projection method in order to increase the overall computational efficiency of the methodology. Application of the framework to large three-dimensional problems is carried out. A series of numerical examples will be presented in order to demonstrate the robustness and flexibility of the proposed methodology.

1 INTRODUCTION

Fluid-Structure Interaction (FSI) has been a major topic of research interest for the past few decades. From the spatial discretisation point of view, two general approaches can be established, namely boundary fitted methods and immersed methods. Boundary fitted methods rely on the coupling of the velocity field at the interface between the two phases describing the problem (i.e. fluid and solid). This coupling can be carried out either in a monolithic manner [1] or in a partitioned staggered manner [2, 3], always requiring the consistent update of the interface and the use of an Arbitrary Lagrangian Eulerian approach to describe the fluid phase.

On the contrary, immersed methods are designed to embed the solid phase within the fluid phase, enabling the calculation of the FSI effect on a stationary fluid grid which can be analysed in a purely Eulerian fashion [4, 5, 6, 7]. From a methodological point of view, immersed methods are part of the so-called Fictitious Domain (FD) philosophy, introduced by Glowinski in [8] for the resolution of boundary value problems in complex geometrical settings.

Three different FD approaches can be identified. First, non-body force based schemes, where the presence of an immersed solid is established by enforcing strongly that the velocity of the surrounding fluid matches that of the immersed structure at the interface (i.e. Dirichlet Boundary Conditions (BCs) on the fluid); in turn, the movement of the immersed solid is obtained after the equation of motion of the solid is solved subjected to the force field imposed by the surrounding fluid domain (i.e. Neumann BCs on the solid). Second, body force based Distributed Lagrange Multiplier (DLM) methods, where the no-slip velocity constraint at the interface between the physics is imposed as an equation for the Lagrange multiplier defined on the solid boundary. Third, body force based non-DLM methods, where the no-slip velocity constraint is imposed strongly on the solid (i.e. Dirichlet BCs on the solid) and a FSI body force is then evaluated and applied to the surrounding fluid (i.e. Neumann BCs on the fluid). Methods such as the Immersed Boundary Method (IBM) [4], the Extended Immersed Boundary Method (EIBM) [9] and the Immersed Finite Element Method [10] belong to this group.

An alternative immersed methodology, named Immersed Structural Potential Method (ISPM), was introduced in [6]. In the ISPM, the kinematics of the solid is completely defined by the underlying fluid domain through suitable interpolating functions and the solid is modelled by means of a deviatoric energy potential which is accurately evaluated at a cloud of integration points. The methodology has been improved in [11] by introducing smoothed spline-based kernels for the definition of the interpolating functions and high order quadrature rules to ensure the accurate description of the solid phase. In this paper, a further improvement is introduced in the form of a Runge-Kutta Chebyshev Projection (RKCP-ISPM) time integration scheme, leading to a very efficient fully parallelised framework that allows for the simulation of large-scale three-dimensional problems.

2 FLUID GOVERNING EQUATIONS

Let us consider the motion of a continuum defined by means of a mapping $\boldsymbol{\phi}$ established between a reference or material configuration $\boldsymbol{X} \in \Omega_0 \subset \mathbb{R}^d$ and a spatial or current configuration $\boldsymbol{x} \in \Omega \subset \mathbb{R}^d$ at time t, namely $\boldsymbol{x}(t) = \boldsymbol{\phi}(\boldsymbol{X}, t)$, where $d = \{2, 3\}$ represents the number of space dimensions. The deformation gradient tensor $\boldsymbol{F}$ is defined as the material gradient of the spatial position as

$$\boldsymbol{F} = \nabla_0 \boldsymbol{x} = \frac{\partial \boldsymbol{x}}{\partial \boldsymbol{X}}, \quad J = \det \boldsymbol{F} \tag{1}$$

where J is the Jacobian of the transformation. In addition, the velocity field $\boldsymbol{u} = [u_1 \dots u_d]^{\mathrm{T}}$ of the continuum is computed as $\boldsymbol{u}(\boldsymbol{X}, t) = \frac{\partial \boldsymbol{x}}{\partial t}$. In the case of an incompressible Newtonian viscous fluid, the conservation of linear momentum for an arbitrary spatial volume Ω of boundary $\delta\Omega$ with outward normal $\boldsymbol{n}$ is expressed in integral form as

$$\int_\Omega \frac{\partial}{\partial t}(\rho \boldsymbol{u}) \, \mathrm{d}v + \int_{\partial\Omega} (\rho \boldsymbol{u} \otimes \boldsymbol{u} + p\boldsymbol{I} - \mu \boldsymbol{\nabla} \boldsymbol{u}) \cdot \boldsymbol{n} \, \mathrm{d}a - \int_\Omega \boldsymbol{g} \, \mathrm{d}v = \boldsymbol{0}, \tag{2}$$

where $\boldsymbol{I}$ is the identity tensor, $\boldsymbol{g}$ denotes an external volume force field per unit of spatial volume, p is the scalar pressure field, μ is the viscosity and ρ the density of the fluid.

Within the framework of low order Finite Volume schemes and particularising for the case of a Cartesian staggered mesh, let $\Omega_{u^{A_i}}, i \in \{1 \dots d\}$ be the control volume associated with the Cartesian component of the trial and test velocity components u^{A_i} and δu^{A_i}, respectively, with an arrangement similar to that of a Marker And Cell (MAC) grid. Here, A_i denotes the fluid control volume face perpendicular to the i-th Cartesian axis and u^{A_i} and δu^{A_i} the corresponding normal trial and test face velocity fields. The Finite Volume semi-discrete weak form of the linear momentum equation reads

$$\int_{\Omega_{u^{A_i}}} \delta u^{A_i} \frac{\partial}{\partial t} \left(\boldsymbol{e}_i \cdot \rho \boldsymbol{u} \right) \, \mathrm{d}v + \int_{\partial \Omega_{u^{A_i}}} \delta u^{A_i} \boldsymbol{e}_i \cdot \boldsymbol{\mathcal{F}} \boldsymbol{n} \, \mathrm{d}a - \int_{\Omega_{u^{A_i}}} \delta u^{A_i} \boldsymbol{e}_i \cdot \boldsymbol{g} \, \mathrm{d}v = 0, \quad i \in \{1 \dots d\} \tag{3}$$

where $\{\boldsymbol{e}_i\}, i \in \{1 \dots d\}$ is the Cartesian unit basis and $\boldsymbol{\mathcal{F}}$ defines the numerical interface flux, namely,

$$\boldsymbol{\mathcal{F}} = \rho \boldsymbol{u} \otimes \boldsymbol{u} + p \boldsymbol{I} - \mu \boldsymbol{\nabla} \boldsymbol{u}. \tag{4}$$

Equation (3) is solved along with the divergence free velocity constraint as part of a fractional step algorithm [12].

3 IMMERSED SOLID GOVERNING EQUATIONS

Let us consider an incompressible deformable solid with density ρ_s fully immersed within the surrounding incompressible viscous fluid. The solid can be modelled as a deviatoric Helmholtz's free energy density functional $\widehat{\Psi}^s$ whose spatial gradient defines a FSI force field which is regarded as an external source term by the background viscous fluid [12].

For spatial semi-discretisation purposes, the solid domain is modelled in a Lagrangian manner as a collection of integration points a_p immersed within the fluid, moving from an initial position $\boldsymbol{X}^{a_p}$ to the spatial position $\boldsymbol{x}^{a_p}$ at time instant t, through the deformation gradient tensor $\boldsymbol{F}$ defined by the motion of the surrounding continuum (i.e. non-slip condition). With the purpose of distinguishing the surrounding fluid phase from the immersed solid phase, a superindex $(.)^s$ will be employed wherever necessary when referring to the latter.

The kinematics of the immersed solid is defined by the underlying fluid domain. Thus, the velocity of the deformable immersed solid can be obtained after suitable definition of an interpolation operator which enables to transfer information from the background Eulerian fluid to the Lagrangian solid. Specifically, the velocity field $\boldsymbol{u}^s$ at any integration point a_p currently at $\boldsymbol{x}^{a_p}$ can be evaluated as follows,

$$\mathcal{I}(\boldsymbol{u})(\boldsymbol{x}^{a_p}) := \boldsymbol{u}^{a_p} = \left[u_1^{a_p} \dots \; u_d^{a_p} \right]^{\mathrm{T}}, \qquad u_i^{a_p} = \sum_{A_i} u^{A_i} \varphi^{A_i} \left(\boldsymbol{x}^{a_p} \right) \tag{5}$$

where

$$\varphi^{A_i}(\boldsymbol{x}^s) = \varphi(\boldsymbol{x}^s - \boldsymbol{x}^{A_i}) \tag{6}$$

are interpolating functions centred at fluid control volume faces A_i, defined by the spatial position $\boldsymbol{x}^{A_i}$, mid-point of the respective fluid control volume face. Similarly, the virtual velocity field vector $\delta\boldsymbol{u}^s$ is evaluated at a structure integration point a_p with a consistent interpolating methodology (7), to ensure conservation of the overall scheme

$$\delta\boldsymbol{u}^{a_p} = \left[\delta u_1^{a_p} \dots \ \delta u_d^{a_p}\right]^{\mathrm{T}}, \qquad \delta u_i^{a_p} = \sum_{A_i} \delta u^{A_i} \varphi^{A_i}\left(\boldsymbol{x}^{a_p}\right). \tag{7}$$

The internal virtual work formulated in the case of the immersed solid domain is defined as the directional derivative of the Helmholtz's free energy functional with respect to a virtual velocity field vector as follows,

$$\delta W_{int}^s(\boldsymbol{\phi}, \delta\boldsymbol{u}^s) = \int_{\Omega_0^s} \boldsymbol{\tau}'^s : \boldsymbol{\nabla}\delta\boldsymbol{u}^s \, \mathrm{d}V \simeq \sum_{a_p} W^{a_p} \boldsymbol{\tau}'^{s,a_p} : \boldsymbol{\nabla}\delta\boldsymbol{u}^{a_p} \tag{8}$$

where $\boldsymbol{\tau}'^s$ is the deviatoric Kirchhoff stress tensor. The evaluation of the above formula (8) requires the computation of the spatial gradient of the virtual velocity at integration point a_p, which can be easily obtained by making use of the spatial gradient of the interpolating functions defined above,

$$\boldsymbol{\nabla}\delta\boldsymbol{u}^{a_p} = \left[\sum_{A_1} \boldsymbol{\nabla}\varphi^{A_1}\left(\boldsymbol{x}^{a_p}\right)\delta u^{A_1} \quad \dots \quad \sum_{A_d} \boldsymbol{\nabla}\varphi^{A_d}\left(\boldsymbol{x}^{a_p}\right)\delta u^{A_d}\right]^T. \tag{9}$$

After re-writing the Kirchhoff stress tensor in the form $\boldsymbol{\tau}'^s = [\boldsymbol{\tau}_1'^s \dots \boldsymbol{\tau}_d'^s]$, equation (8) can be reformulated in a discrete manner as

$$\delta W_{int}^s(\boldsymbol{\phi}, \delta\boldsymbol{u}^s) = \sum_{A_1} \delta u_{A_1} f_{A_1} + \dots + \sum_{A_d} \delta u_{A_d} f_{A_d} \tag{10}$$

where

$$f_{A_i} = \int_{\Omega_0^s} \boldsymbol{\tau}_i'^s \cdot \boldsymbol{\nabla}\varphi^{A_i}(\boldsymbol{x}^s) \, \mathrm{d}V \simeq \sum_{a_p} W^{a_p} \boldsymbol{\tau}_i'^{s,a_p} \cdot \boldsymbol{\nabla}\varphi^{A_i}(\boldsymbol{x}^{a_p}), \quad i \in \{1 \dots d\} \tag{11}$$

In order to guarantee conservation of the scheme it transpires that

$$g_{A_i} := \int_{\Omega_{u^{A_i}}} \boldsymbol{e}_i \cdot \boldsymbol{g} \, \mathrm{d}v = \frac{f_{A_i}}{|\Omega_{u^{A_i}}|} \tag{12}$$

where g_{A_i} represents the FSI force per unit volume $|\Omega_{u^{A_i}}|$ which must be applied at the fluid control volume face A_i. A key ingredient for the evaluation of the stress tensor $\boldsymbol{\tau}'^s$ is

the deformation gradient tensor $\boldsymbol{F}$ at any location within the immersed continuum. First, the spatial velocity gradient tensor $\boldsymbol{l}$ is evaluated at every integration point a_p, for which the following interpolation operator is used

$$\boldsymbol{\nabla}\mathcal{I}(\boldsymbol{u})(\boldsymbol{x}^{a_p}) := \boldsymbol{l}^{a_p} = \boldsymbol{\nabla}\boldsymbol{u}^{a_p} = \left[\sum_{A_1} \boldsymbol{\nabla}\varphi^{A_1}\left(\boldsymbol{x}^{a_p}\right) u^{A_1} \quad \dots \quad \sum_{A_d} \boldsymbol{\nabla}\varphi^{A_d}\left(\boldsymbol{x}^{a_p}\right) u^{A_d}\right]^T \tag{13}$$

where the spatial gradient of the interpolating functions $\{\boldsymbol{\nabla}\varphi^{A_x},\ \boldsymbol{\nabla}\varphi^{A_y}\}$ can be explicitly computed. Second, a time integration scheme is proposed for the tensor system of kinematic differential equations

$$\dot{\boldsymbol{F}} = \boldsymbol{l}\boldsymbol{F} = (\boldsymbol{d} + \boldsymbol{w})\,\boldsymbol{F} \tag{14}$$

where $\boldsymbol{d}$ and $\boldsymbol{w}$ are the strain rate tensor and the vorticity tensor, respectively. An iterative explicit time integration scheme can be employed with the purpose of obtaining $\boldsymbol{F}$ at time instant $n+1$ and iteration $k+1$ as

$$\boldsymbol{F}^{n+1}_{k+1} = e^{\Delta t \boldsymbol{l}^{n+1}_{k+1}} \boldsymbol{F}^{n}. \tag{15}$$

A suitable $\boldsymbol{d}$-$\boldsymbol{w}$ structure preserving time integration scheme is presented in [12] in order to ensure the volume conservation of the immersed solid phase. In addition, the introduction of smoothed spline-based kernels for the evaluation of the interpolating functions φ^{A_i} leads to improved shear stresses in the immersed solid phase [11]. From the close-ups in Figure 1 it can be noted how the combination of the ISPM with the new kernel 'k15' removes most of the oscillations present in $\boldsymbol{F}$, which are present in both the EIBM and ISPM while using existing Peskin's kernels [4]. Furthermore, the use of high order quadrature rules used to discretise the immersed solid phase ensures the accurate description of the solid phase, preventing the so-called numerical leakage [11].

4 EXPLICIT RUNGE-KUTTA-CHEBYSHEV-PROJECTION METHOD

Runge-Kutta-Chebyshev (RKC) methods are a subclass of explicit Runge-Kutta (RK) methods, where instead of trying to maximise the order of the method for a given number of stages, as it is customary for typical RK methods, only the first two stages are used to ensure second order accuracy, and the remaining stages are used to maximise the region of absolute stability of the method, while keeping an explicit scheme with low storage requirements. In the case of RKC methods, this is achieved by careful choice of the constants so that the stability polynomials can be expressed in terms of Chebyshev polynomials. The well known three-term recurrence equation that these polynomials satisfy translates also to three-term recurrence relations for stage updates.

This choice of time integrator has been favoured for the ISPM framework as the second order accuracy in time is in agreement with the errors incurred by the spatial semi-discretisation, but also because it minimises the number of intermediate vectors that

have to be stored while providing extra stability, a highly desirable feature for fluid-structure interaction problems given their multiple sources of non-linearity. The original RKC method was introduced by Van der Houwen [13] and extended to the use with projection methods (RKCP) by Zheng and Petzold [14] for incompressible flow with no solid interaction. In this section, a combination of the RKCP with the ISPM is presented (RKCP-ISPM).

In order to ease the exposition, it will be convenient to recast the problem in the notation that is classical in the context of ODE integrators. To this purpose, we rewrite the governing equations in the form

$$\dot{\boldsymbol{Y}} = \boldsymbol{f}(t, \boldsymbol{Y}); \quad \boldsymbol{Y} = \left[\begin{array}{c} \boldsymbol{Y}_1 \\ \boldsymbol{Y}_2 \\ \boldsymbol{Y}_3 \end{array} \right] = \left[\begin{array}{c} \boldsymbol{u} \\ \boldsymbol{F} \\ \boldsymbol{x} \end{array} \right] \tag{16}$$

where

$$f(t, \boldsymbol{Y}) = \left[\begin{array}{c} -(\boldsymbol{Y}_1 \cdot \nabla)\boldsymbol{Y}_1 + \frac{\mu}{\rho}\Delta \boldsymbol{Y}_1 - \frac{1}{\rho}\nabla p + \frac{1}{\rho}\boldsymbol{g}(\boldsymbol{Y}, t) \\ \nabla \mathcal{I}(\boldsymbol{Y}_1)\boldsymbol{Y}_2 \\ \mathcal{I}(\boldsymbol{Y}_1)(\boldsymbol{Y}_3, t) \end{array} \right] \tag{17}$$

Note how in the above equations, the first term corresponds to the incompressible Navier-Stokes equations, whereas the second accounts for the integration of the deformation gradient using the interpolated velocity gradient and the third for the integration of the position of the quadrature nodes using the interpolated velocity field.

With the above notation, we can pose the following s-stage explicit RKCP integration scheme coupled with the ISPM. In the formulas that follow, $\boldsymbol{Y}_{j,k}$ denotes the value of the k-th variable of the system for stage j. For the initial stage ($j = 0$) we have

$$\left\{ \begin{array}{l} \boldsymbol{Y}_{0,1} = \boldsymbol{u}^n, \\ \boldsymbol{Y}_{0,2} = \boldsymbol{F}^n, \\ \boldsymbol{Y}_{0,3} = \boldsymbol{x}^{a_p,n} \end{array} \right. \tag{18}$$

The first stage advances in time as follows,

$$\left\{ \begin{array}{l} \boldsymbol{Y}_{1,2} = e^{c_0 \Delta t \mathcal{Q}(\nabla \mathcal{I}(\boldsymbol{Y}_{0,1})(\boldsymbol{Y}_{0,3}))}\boldsymbol{Y}_{0,2}, \\ \boldsymbol{Y}_{1,3} = \boldsymbol{x}^{a_p,n} + \tilde{\mu}_1 \Delta t \mathcal{I}(\boldsymbol{Y}_{0,1})(\boldsymbol{Y}_{0,3}), \\ \bar{\bar{\boldsymbol{F}}}_{0,1} = -(\boldsymbol{u}^n \cdot \nabla_h)\boldsymbol{u}^n + \frac{\mu}{\rho}\Delta_h \boldsymbol{u}^n - \frac{1}{\rho}\nabla_h p_n + \boldsymbol{f}_h^0(\boldsymbol{u}^n, \boldsymbol{x}^{a_p,n}, t, \boldsymbol{F}^n), \\ \boldsymbol{Y}_{1,1}^* = \boldsymbol{u}^n + \tilde{\mu}_1 \Delta t \bar{\bar{\boldsymbol{F}}}_{0,1}, \\ \boldsymbol{Y}_{1,1} = \mathcal{P}(\boldsymbol{Y}_{1,1}^*) \end{array} \right. \tag{19}$$

where in the above ∇_h and Δ_h denote the corresponding discretised versions of the gradient and Laplacian operators, and the interaction force term is defined as

$$f_{i,h}^0 = \int_{\Omega_0^s} \boldsymbol{\tau}_i'^s(\boldsymbol{Y}_{1,2}) \cdot \boldsymbol{\nabla} \varphi^{A_i}(\boldsymbol{Y}_{0,3}) \, \mathrm{d}V + (\rho_s - \rho) \frac{\mathcal{I}(\boldsymbol{Y}_{0,1})(\boldsymbol{Y}_{0,3}) - \mathcal{I}(\boldsymbol{u}^{n-1})(\boldsymbol{x}^{n-1})}{\Delta t} \tag{20}$$

Note that in the first equation in (19) the deformation gradient is integrated to obtain a deformation gradient for the stage to evaluate the forces arising from (20). The second equation in (19) integrates the position of the quadrature nodes, and the remaining equations apply the fractional step method to solve the incompressible Navier-Stokes equations.

For stage j we have analogously

$$\left\{\begin{array}{l}\boldsymbol{Y}_{j,2}=e^{c_j\Delta t\mathcal{Q}(\nabla\mathcal{I}(\boldsymbol{Y}_{j-1,1})(\boldsymbol{Y}_{j-1,3}))}\boldsymbol{Y}_{0,2},\\ \boldsymbol{Y}_{1,3}=(1-\mu_j-\nu_j)\boldsymbol{x}^{a_p,n}+\mu_j\boldsymbol{Y}_{j-1,3}+\nu_j\boldsymbol{Y}_{j-2,3}+\tilde{\mu}_j\Delta t\mathcal{I}(\boldsymbol{Y}_{j-1,1})(\boldsymbol{Y}_{j-1,3})+\tilde{\gamma}_j\Delta t\mathcal{I}(\boldsymbol{Y}_{0,1})(\boldsymbol{Y}_{0,3}),\\ \bar{\bar{\boldsymbol{F}}}_{j-1,1}=-(\boldsymbol{Y}_{j-1,1}\cdot\nabla_h)\boldsymbol{Y}_{j-1,1}+\frac{\mu}{\rho}\Delta_h\boldsymbol{Y}_{j-1,1}-\frac{1}{\rho}\nabla_h p_n+\boldsymbol{f}_h^{j-1}(\boldsymbol{Y}_{j-1,1},\boldsymbol{Y}_{j-1,3},t+c_{j-1}\Delta t,\boldsymbol{Y}_{j,2}),\\ \boldsymbol{Y}^*_{j,1}=(1-\mu_j-\nu_j)\boldsymbol{Y}_{0,1}+\mu_j\boldsymbol{Y}_{j-1,1}+\nu_j\boldsymbol{Y}_{j-2,1}+\tilde{\mu}_j\Delta t\bar{\bar{F}}_{j-1,1}+\tilde{\gamma}_j\Delta t\bar{\bar{F}}_{0,1},\\ \boldsymbol{Y}_{j,1}=\mathcal{P}(\boldsymbol{Y}^*_{j,1})\end{array}\right. \tag{21}$$

where

$$f_{i,h}^{j-1}=\int_{\Omega_0^s}\boldsymbol{\tau}_i'^s(\boldsymbol{Y}_{j,2})\cdot\boldsymbol{\nabla}\varphi^{A_i}(\boldsymbol{Y}_{j-1,3})\,\mathrm{d}V+(\rho_s-\rho)\frac{\mathcal{I}(\boldsymbol{Y}_{j-1,1})(\boldsymbol{Y}_{j-1,3})-\mathcal{I}(\boldsymbol{Y}_{0,1})(\boldsymbol{Y}_{0,3})}{c_{j-1}\Delta t} \tag{22}$$

In order to complete the fractional step method, the operator $\mathcal{P}$ is defined as

$$\mathcal{P}(\boldsymbol{u}^*)=\boldsymbol{u}^*-\nabla\phi \tag{23}$$

where ϕ is the solution of following Poisson's problem

$$\left\{\begin{array}{rcl}\Delta\phi & = & \nabla\cdot\boldsymbol{u}^*,\ \text{in}\ \Omega\\ \nabla\phi\cdot\boldsymbol{n} & = & 0,\ \text{on}\ \partial\Omega\end{array}\right. \tag{24}$$

And in order to ensure that the integration scheme used for component $\boldsymbol{Y}_2$ preserves the incompressibility constraint, the operator $\mathcal{Q}$ is defined as the projection onto traceless tensors as follows

$$\mathcal{Q}(\boldsymbol{l})=\boldsymbol{l}-\frac{1}{d}\left(\boldsymbol{I}\otimes\boldsymbol{I}\right):\boldsymbol{l} \tag{25}$$

for $d=3$ and by

$$\mathcal{Q}(\boldsymbol{l})=\left[\begin{array}{ccc}\frac{1}{2}(l_{11}-l_{22}) & l_{12} & 0\\ l_{21} & \frac{1}{2}(l_{22}-l_{11}) & 0\\ 0 & 0 & 0\end{array}\right] \tag{26}$$

for $d=2$, being d the number of space dimensions. The scalar constants in the stage recurrence relations are defined by

$$\begin{array}{l}c_0=0,\quad c_1=c_2,\quad c_2=\tilde{\mu}_1,\quad c_j=\frac{T_s'(\omega_0)}{T_s''(\omega_0)}\cdot\frac{T_j''(\omega_0)}{T_j'(\omega_0)},\ j=3,\ldots,s\\ b_0=\frac{1}{4\omega_0^2},\quad b_1=\frac{1}{\omega_0},\quad b_j=\frac{T_j''(\omega_0)}{T_j'(\omega_0)^2},\ j=2,\ldots,s\\ \mu_j=2\omega_0 b_j/b_{j-1},\quad \tilde{\mu}_j=\mu_j\omega_1/\omega_0,\quad \tilde{\gamma}_{j-1}=(T_{j-1}(\omega_0)b_{j-1}-1)\mu_j\frac{\omega_1}{\omega_0},\ j=1,\ldots,s\\ \nu_j=-b_j/b_{j-2},\ j=2,\ldots,s,\quad \omega_0=1+\frac{\varepsilon}{s^2},\quad \omega_1=\frac{T_s'(\omega_0)}{T_s''(\omega_0)}\end{array} \tag{27}$$

so that the corresponding stability polynomial is

$$P_j(z) = a_j + b_j T_j(\omega_0 + \omega_1 z), \text{ where } \quad a_j = -\tilde{\gamma}_j/\tilde{\mu}_j \tag{28}$$

In all the above T_j denotes the $j-th$ Chebyshev polynomial of the first kind and the damping parameter ε is chosen as $2/13$. The choice for b_0 and b_1 in the formulas above is carried out as recommended in [15] for advection-diffusion-reaction problems. It is worth mentioning that this approach is not a mere application of the RKCP method to fluid-structure interaction using ISPM. The component $\boldsymbol{Y}_2$ of the system vector is not integrated using the RKC scheme, but updated using the explicit structure-preserving scheme introduced in [12]. The use of this integrator ensures the satisfaction of the incompressibility constraint in the solid exactly.

5 NUMERICAL RESULTS

In this section we present a large-scale numerical example solved using the above presented methodology. We consider a prismatic channel $\Omega = [0,8] \times [0,2] \times [0,2]$ filled with an incompressible fluid of density $\rho = 1$ and viscosity $\mu = 5 \cdot 10^{-3}$ and five flexible membranes $\Omega_i^s,\ i = 1, \ldots, 5$ of density $\rho = 1$ and dimensions $0.2 \times 1.5 \times 1$ uniformly spaced and centred along the channel (separated by a distance of 1). The membranes obey a Neo-hookean material model with shear modulus $G = 3.846 \cdot 10^4$. All boundaries are set to a non-slip boundary condition, except for the short ends, where a Poiseuille pulsatile flow of amplitude $A = 5(\sin(2\pi t) + 1.1)$ is applied (left end) and outflow boundary conditions (right end). Note that due to the boundary condition, the flow always goes from left to right, with different positive velocity. The fluid is discretised using a staggered Finite Volume scheme with $256 \times 64 \times 64$ control volumes and adaptive time-step using the RKCP presented in the previous section ($s = 10$). The solid membranes are integrated using a composite Gaussian quadrature rule of degree 6 in each direction with $2 \times 11 \times 8$ subintervals (giving a total of 38016 integration points per membrane).

As it can be observed in Figures 2 and 3, a complex flow pattern develops around the membranes and causes them to deform. The always right-flowing fluid exerts a force on the first membrane, which stays deformed during the whole cycle. The rest of the membranes oscillate depending on the formation of vortices downstream as the flow decelerates (see amplitude function).

The above example has been solved using a hybrid Matlab/Fortran implementation where the computation of forces is parallelised using OpenMP. The total number of fluid variables is close to 3.2 million, and the solid discretisation is short of 0.2 million integration points. The runtime on a i7-2760QM processor is around 20 hours per amplitude cycle.

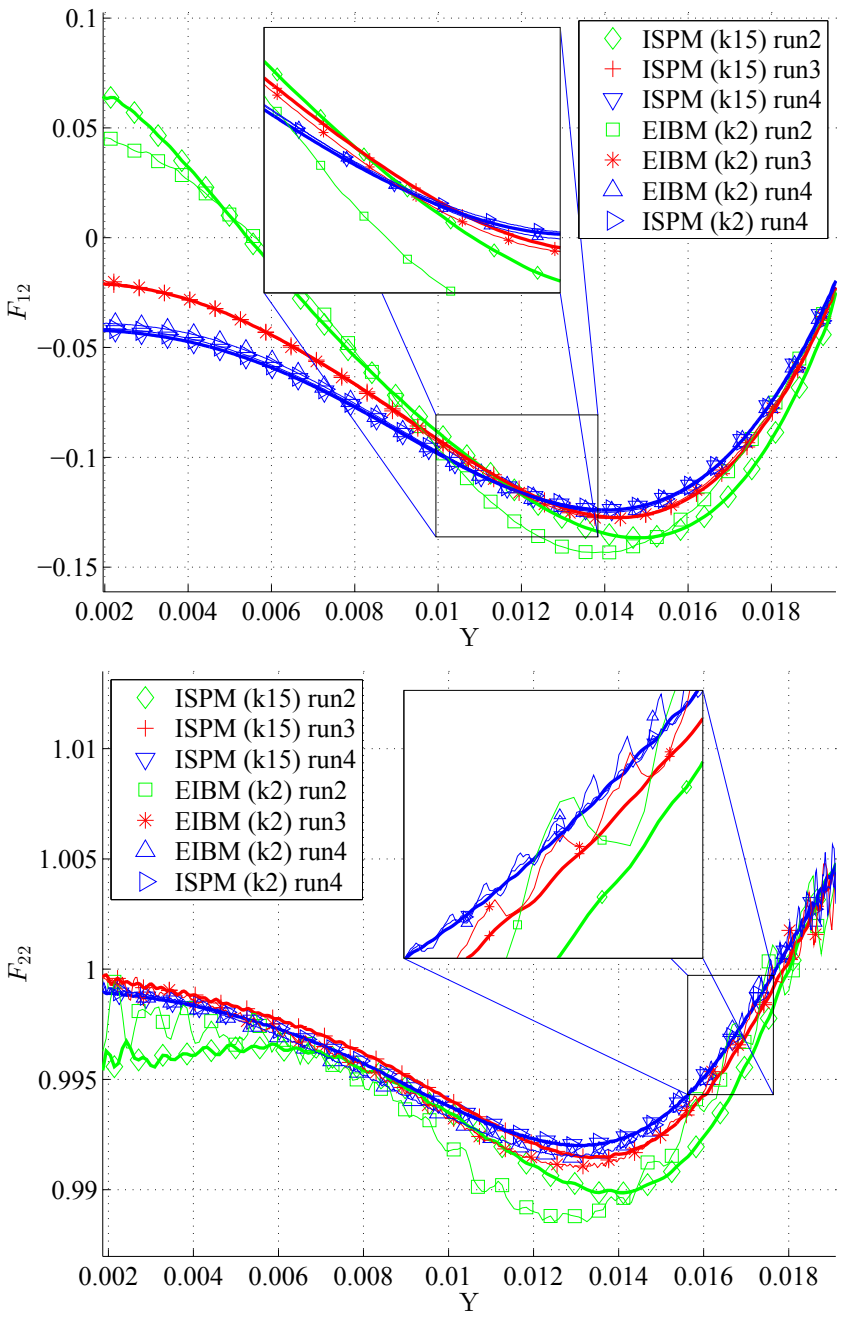

Figure 1: Deformation gradient tensor components F_{12} and F_{22} for the leading edge of an immersed membrane (as seen with respect to the material coordinates) for a model problem [11]. Thick lines represent solutions obtained with the ISPM and an improved kernel 'k15' for different mesh refinements (runs 2, 3 and 4 in increasing order of refinement). Thin lines represent corresponding solutions obtained with the EIBM and Peskin's kernel ('k2'). The solution obtained with the ISPM and Peskin's kernel and the finest mesh has also been added to allow for comparison with the original ISPM. Note that equal line colours correspond to the same discretisation level.

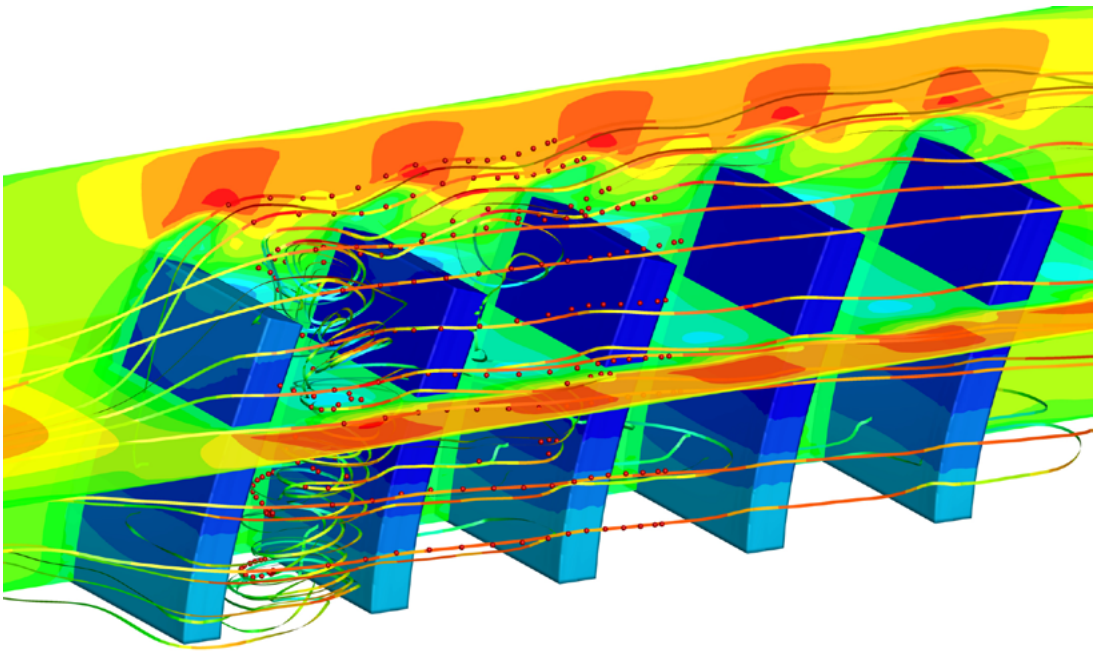

Figure 2: Streamlines, deformation and flow slices at $t = 0.28$s. Contour colors correspond to horizontal component of fluid/solid velocity. Red spherical markers are passive flow tracers.

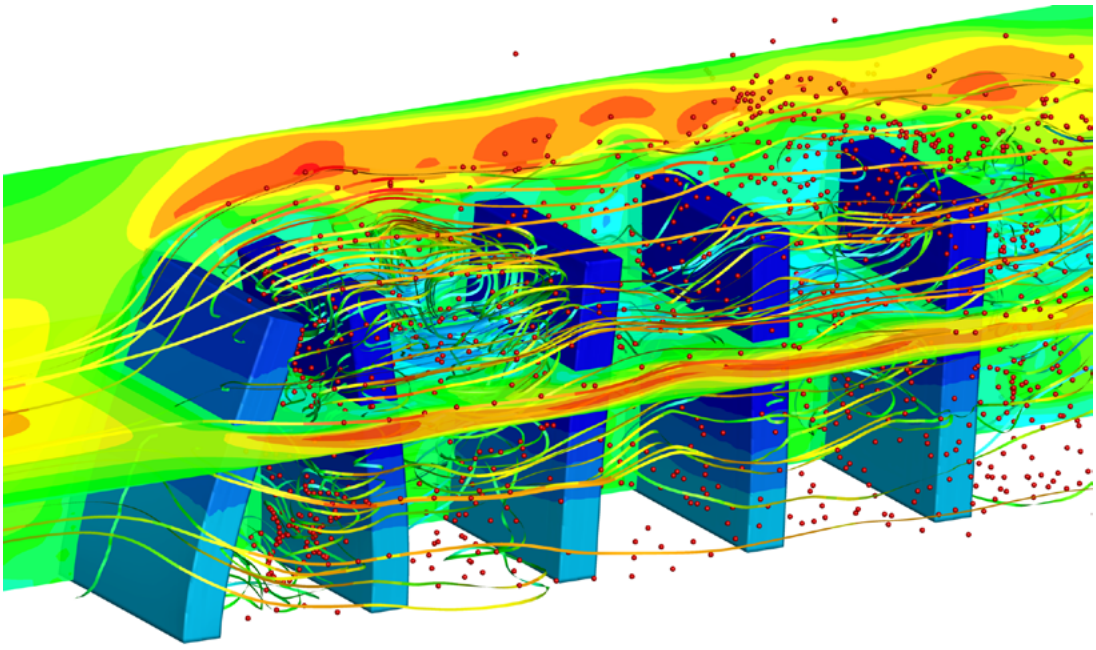

Figure 3: Streamlines, deformation and flow slices at $t = 2.44$s. Contour colors correspond to horizontal component of fluid/solid velocity. Red spherical markers are passive flow tracers.

REFERENCES

[1] T. Tezduyar. Finite element methods for flow problems with moving boundaries and interfaces. *Arch. Comput. Methods Engrg.*, 8:83–130, 2001.

[2] C. Wood, A. J. Gil, O. Hassan, and J. Bonet. Partitioned block- Gauss- Seidel coupling for dynamic fluid-structure interaction. *Computers and Structures*, 2008. DOI: 10.1016/j.compstruc.2008.08.005.

[3] C. Wood, A. J. Gil, O. Hassan, and J. Bonet. A partitioned coupling approach for dynamic fluid-structure interaction with applications to biological membranes. *International Journal for Numerical Methods in Fluids*, 57(5):555–581, 2008. DOI: 10.1002/fld.1815.

[4] C. Peskin. The immersed boundary method. *Acta Numerica*, 11:479–517, 2002.

[5] X. Wang and W. Liu. Extended immersed boundary method using FEM and RKPM. *Comput. Methods Appl. Mech. Engrg.*, 193:1305–1321, 2004.

[6] A. Gil, A. Arranz Carreño, J. Bonet, and O. Hassan. The immersed structural potential method for haemodynamic applications. *Journal of Computational Physics*, 229:8613–8641, 2010.

[7] C. Hesch, A. Gil, A. Arranz Carreño, and J. Bonet. On immersed techniques for fluid-structure interaction. *Comput. Methods Appl. Mech. Engrg.*, 247-248:51–64, 2012.

[8] R. Glowinski, T.-W. Pan, and J. Périaux. A fictitious domain method for Dirichlet problems and applications. *Computer Methods in Applied Mechanics and Engineering*, 111:283 – 303, 1994.

[9] X. Wang and W. K. Liu. Extended immersed boundary method using FEM and RKPM. *Computer Methods in Applied Mechanics and Engineering*, 193(12-14):1305–1321, 2004. Meshfree Methods: Recent Advances and New Applications.

[10] W. K. Liu, D. W. Kim, and S. Tang. Mathematical foundations of the immersed finite element method. *Computational Mechanics*, 39(3):211–222, 2007.

[11] A. J. Gil, A. Arranz Carreño, J. Bonet, and O. Hassan. An enhanced Immersed Structural Potential Method for fluid–structure interaction. *Journal of Computational Physics*, 2012. submitted.

[12] A. J. Gil, A. Arranz Carreño, J. Bonet, and O. Hassan. The Immersed Structural Potential Method for haemodynamic applications. *Journal of Computational Physics*, 229(22):8613–8641, 2010.

[13] P. J. van Der Houwen and B. P. Sommeijer. On the Internal Stability of Explicit, m-Stage Runge-Kutta Methods for Large m-Values. *ZAMM - Zeitschrift für Angewandte Mathematik und Mechanik*, 60(10):479–485, 1980.

[14] Z. Zheng and L. Petzold. Runge-Kutta-Chebyshev projection method. *Journal of Computational Physics*, 219(2):976 – 991, 2006.

[15] J. G. Verwer, B. P. Sommeijer, and W. Hundsdorfer. RKC time-stepping for advection-diffusion-reaction problems. *Journal of Computational Physics*, 201(1):61 – 79, 2004.